

The origins of pressure-induced phase transformations during the surface texturing of silicon using femtosecond laser irradiation

Matthew J. Smith,¹ Meng-Ju Sher,² Benjamin Franta,³ Yu-Ting Lin,³ Eric Mazur,^{2,3} and Silvija Gradečak¹

¹*Department of Materials Science and Engineering, Massachusetts Institute of Technology, Cambridge, Massachusetts 02139, USA*

²*Department of Physics, Harvard University, Cambridge, Massachusetts 02138, USA*

³*School of Engineering and Applied Sciences, Harvard University, Cambridge, Massachusetts 02138, USA*

(Received 27 July 2012; accepted 19 September 2012; published online 22 October 2012)

Surface texturing of silicon using femtosecond (fs) laser irradiation is an attractive method for enhancing light trapping, but the laser-induced damage that occurs in parallel with surface texturing can inhibit device performance. In this work, we investigate the light-material interaction during the texturing of silicon by directly correlating the formation of pressure-induced silicon polymorphs, fs-laser irradiation conditions, and the resulting morphology and microstructure using scanning electron microscopy, micro-Raman spectroscopy, and transmission electron microscopy. We show that raster scanning a pulsed laser beam with a Gaussian profile enhances the formation of crystalline pressure-induced silicon polymorphs by an order of magnitude compared with stationary pulsed fs-laser irradiation. Based on these observations, we identify resolidification-induced stresses as the mechanism responsible for driving sub-surface phase transformations during the surface texturing of silicon, the understanding of which is an important first step towards reducing laser-induced damage during the texturing of silicon with fs-laser irradiation. © 2012 American Institute of Physics. [<http://dx.doi.org/10.1063/1.4759140>]

I. INTRODUCTION

The irradiation of silicon with pulsed femtosecond (fs) laser irradiation has many advantages as a platform for both the surface-texturing and hyperdoping of silicon for optoelectronic applications.¹ The ablation processes that drive surface texturing during fs-laser irradiation produce uniform texturing on multi-crystalline silicon solar cells,^{2–4} the periodicity and dimensions of the surface texture can be controlled through careful selection of the irradiation parameters (e.g., pulse wavelength, duration, fluence, pulse number, or ambient gas), and the resulting texture is highly reproducible.¹ The laser process is dry (as opposed to wet chemical etches), can be incorporated inline, and uses less material than wet chemical etches.⁴ Finally, the micrometer-scale surface morphology achieved through pulsed laser irradiation, formed through interrelated melting and ablation processes over multiple laser pulses,⁵ is effective at reducing reflectivity from the UV to IR.² The ability to improve solar cell performance using pulsed-laser surface texturing has been demonstrated both in academic laboratories^{2,3} and commercially.⁴

In addition to surface texturing, fs-laser irradiation is also of interest as a platform for optical hyperdoping, a process in which pulsed laser irradiation is used to drive ultra-high concentrations of dopants into a material.^{1,6} The fs-laser irradiation of silicon in the presence of chalcogens (S, Se, Te) has been shown to modify the band structure^{7–9} and produce silicon-based IR photodiodes with responsivities extending beyond 0.8 eV.¹⁰ Furthermore, the ability to dope to concentrations orders of magnitude above the solubility limit is a viable route to synthesizing an impurity-band semiconductor.^{11,12}

One important side effect of using fs-laser irradiation in optoelectronic applications, both for surface texturing and optical hyperdoping, is the irradiation-induced damage that can also occur, such as defects, stacking faults, and phase transformations. Damage that occurs on the surface during texturing, whether by fs-laser irradiation² or other techniques,^{13–15} can be removed by subsequent etching and surface passivation, but sub-surface damage is more difficult to remove and can still lead to a reduction in carrier lifetime.¹⁵ Our previous investigations demonstrated that the texturing of the surface of silicon during fs-laser irradiation can occur in parallel with pressure-induced phase transformations, resulting in the formation of amorphous silicon (a-Si) and crystalline silicon polymorphs Si-XII and Si-III¹⁶ beneath the surface. These phases are metastable products of an irreversible phase transformation that silicon undergoes at pressures above 10–12 GPa. Above such pressures silicon transforms from its diamond cubic phase (Si-I) to a β -Sn phase (Si-II), but cannot transform directly back to Si-I upon pressure release. The series of subsequent phase transformations that occurs upon pressure release depends strongly on the pressure unloading conditions;^{17,18} with sufficiently slow pressure unloading, Si-II transforms into an R8 structure (Si-XII), and then reversibly transforms to a BC8 structure (Si-III) around 2 GPa.¹⁹ The formation of Si-XII, however, can be kinetically suppressed by sufficiently fast pressure unloading rates such that fast pressure unloading favors the formation of a-Si over Si-XII and Si-III.²⁰

There are multiple mechanisms by which fs-laser irradiation can generate pressures sufficient to drive the phase transformation.^{21,22} First, heating of the substrate during fs-laser irradiation occurs so quickly that the material is

heated under constant volume, leading to thermoelastic pressure generation on the order of GPa.²³ Second, at high enough energies, the surface layer of the target is completely atomized and expands at high speeds resulting in the ejection of an ionic plasma.²⁴ The expansion of the ionic plasma drives a recoil shock wave into the substrate²⁵ that can reach pressures of tens of GPa.²⁶ Finally, laser-induced melting and resolidification is a well-documented source of stress in semiconductors,²² and the resolidification of molten silicon on a roughened surface during laser irradiation also generates residual stresses in silicon in the GPa range.^{27,28}

Sub-surface phase transformations in silicon have only recently been identified as the product of pressure cycles induced by fs-laser irradiation.¹⁶ Understanding the mechanisms driving sub-surface plastic deformation is thus critical for minimizing or preventing laser-induced damage during fs-laser surface texturing. In this work, we identify the pressure-generation mechanism responsible for driving sub-surface phase transformations in silicon during fs-laser irradiation by directly correlating the formation and distribution of pressure-induced phases with the irradiation conditions at the surface and the resulting surface morphology and microstructure. In addition, the sensitivity of Si-XII and Si-III formation to temperature pressure provides additional insights into the conditions at the surface during fs-laser irradiation.

II. EXPERIMENTAL

We irradiated silicon (100) wafers with focused Ti:sapphire fs-laser pulses ($\lambda = 800$ nm, $\tau = 80$ fs, 25 Hz) at normal incidence in a nitrogen ambient with a pressure of 6.7×10^4 Pa. The fs-laser beam used in this investigation has a Gaussian fluence profile, $F(x, y)$, described by the expression

$$F(x, y) = F_0 e^{-\frac{x^2}{2\sigma_x^2} - \frac{y^2}{2\sigma_y^2}}. \quad (1)$$

Here F_0 is the peak fluence and the parameter σ_i ($i = x$ or y) is related to the full-width-half-maximum, w , by

$$w_i = 2\sqrt{2 \ln(2)} \cdot \sigma_i. \quad (2)$$

A CCD camera was used to precisely measure the intensity profile and the resulting spatial distribution of the fluence (energy density) received by the sample surface. The laser spot size ($w_x \times w_y$) used in this work was $370 \times 470 \mu\text{m}^2$ and the desired laser fluence was achieved by adjusting the output energy of the laser while keeping the spot size the same. We fabricated three sets of samples with different combinations of laser peak fluence and scanning conditions. First, an areal raster sample was fabricated by raster-scanning the laser beam across a $10 \times 10 \text{ mm}^2$ area at peak fluence of 4 kJ/m^2 . Second, to isolate the effect of fluence, stationary irradiated spots were fabricated; each spot received 88 pulses with peak fluence ranging from 1.6 to 4 kJ/m^2 . Last, to isolate the effect of scanning, the laser beam was held stationary but the fluence of subsequent laser pulses was modulated to mimic the irradiation dose received of an areal raster sample. For reference, the single-shot abla-

tion threshold is $3\text{--}4 \text{ kJ/m}^2$ ^{29,30} and the single-shot melting threshold is $\sim 2 \text{ kJ/m}^2$,³¹ but these thresholds are very sensitive to irradiation conditions and decrease with increasing irradiation.³²

Micro-Raman spectroscopy was used to detect the presence of high-pressure silicon phases by monitoring the appearance of the most pronounced Si-XII and Si-III modes. All Raman spectra were collected under the conditions that minimize instrument-based variations and enable qualitative comparison between samples. We used a micro-Raman spectrometer with a 10-mW 632.8-nm HeNe laser, recorded through a $20\times$ objective (0.4 NA) with a spot size of $10 \mu\text{m}$, and projected onto a CCD using a 1200-grooves/mm diffraction grating. Under these conditions, we estimate the depth probed using Raman to be $3 \mu\text{m}$, based on the absorption depth of silicon at 632.8 nm. The relative amounts of Si-XII and Si-III were approximated by comparing the peak intensity (area under each peak after background subtraction), which was determined using RENISHAW WIRE 3.0 software. In order to understand the irradiation conditions favoring Si-XII and Si-III formation, the distribution of silicon polymorphs was spatially mapped across laser-irradiated spots using a programmable stage, providing insight into fluence dependence of polymorph formation during stationary laser-beam irradiation. Raman line scans were collected with a $5 \mu\text{m}$ step size, perpendicular to the direction of laser polarization.

The surface morphology was imaged using the InLens detector of a Zeiss Field Ultra55 field emission scanning electron microscopy (FESEM) operating at 5 kV. Cross-sectional transmission electron microscopy (TEM) samples were prepared using the lift-out method on a FEI Helios 600 dual-beam focused ion beam (FIB). Bright-field (BF) TEM micrographs and selected area diffraction patterns were collected with a JEOL 2011 TEM operated at 200 kV.

III. RESULTS

A. Effect of fs-laser beam rastering on silicon polymorph formation

To elucidate the pressure generation mechanism driving sub-surface phase transformations, direct correlations between irradiation conditions and silicon polymorph formation is critical. When a sample is irradiated by a stationary laser beam with a Gaussian profile, the sample receives irradiation at a constant fluence (Figure 1(a)) that can be determined by measuring the distance from the center of the laser spot and applying Eq. (1). The resulting irradiation conditions at a given point on the surface can be illustrated in a fluence-shot number plot, as illustrated in Figure 1(b) for different points within the irradiated region. In contrast to stationary laser spot irradiation, rastering the pulsed laser beam across the surface—conditions commonly used to texture large areas using fs-laser irradiation—result in more complex irradiation conditions at the surface. The irradiation conditions generated during laser rastering can be condensed into a single term, *shots per area* (s/a), which describes the number of laser pulses received at a single spot with intensity

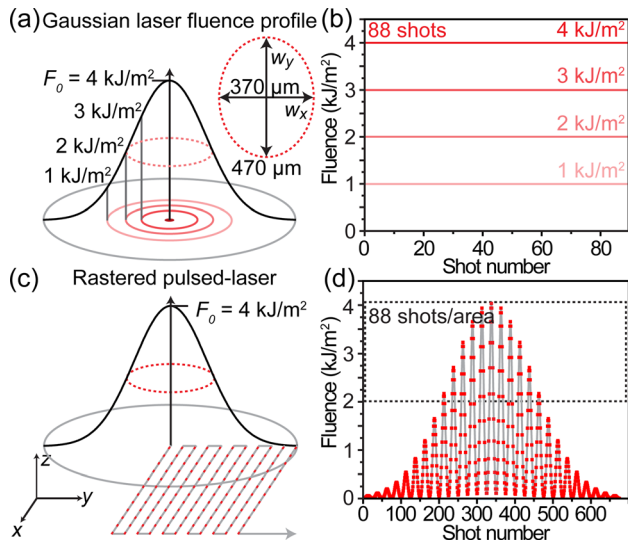


FIG. 1. (a) Schematic of the Gaussian laser fluence profile used in this study, inset shows the (anisotropic) full-width-half-maximum. (b) A fluence-shot number plot showing the irradiation received within the laser spot with increasing distance from the center. (c) Schematic of a rastered Gaussian pulsed-laser beam used to prepare the 88 s/a sample. (d) The fluence of the fs-laser irradiation received at a single point on the surface as the laser spot is rastered over a 2-D area. Dashed box illustrates definition of term *s/a*.

F that satisfy $F_0/2 \leq F \leq F_0$. The shots per area can be written as³³

$$s/a = \frac{\pi w_x w_y}{4 \Delta_x \Delta_y} = \frac{f \pi w_x w_y}{4 v \Delta_y}. \quad (3)$$

Here v is the translation speed, and f is the repetition rate. In this investigation, the laser was scanned in the x -direction (which is also the direction of E-field polarization) with step size $\Delta_x = v/f$ across the desired distance and then stepped perpendicularly a single increment, Δ_y , before being translated back along the x -axis (Figure 1(c)).

Reporting laser rastering in *s/a* has been widely adopted because of its ease of use, but it should be emphasized that this unit does not comprehensively describe the irradiation conditions at the surface during laser rastering. For example, Figure 1(d) illustrates the fluences received by a single point on the surface during the rastering of a 4 kJ/m^2 peak fluence laser beam under conditions corresponding to 88 s/a, the most common irradiation conditions used in this investigation. While a single spot on the surface receives 88 pulses in the range $2\text{--}4 \text{ kJ/m}^2$, the same spot also receives over 300 pulses in the range $0.1\text{--}2 \text{ kJ/m}^2$. Comparing Figures 1(b) and 1(d) illustrates the difference between rastering a pulsed fs-laser beam over the surface and holding it stationary. These differences in irradiation conditions induced by translation of the stage during fs-laser irradiation will prove to be an important component of this investigation.

Using a Gaussian laser beam with a peak fluence of 4 kJ/m^2 , we investigate the pressure-induced phase transformations on a surface that received rastered pulsed laser irradiation (88 s/a) and compare this result with a spot that received 88 pulses from a stationary laser beam. A representative Raman spectrum from the 88 s/a rastered surface (Figure 2(a))

shows well-defined Si-XII and Si-III modes, and their average intensities are shown in Figure 2(b). Micron-scale surface roughness has developed (Figure 2(b), inset) that is characteristic of silicon irradiated with fs-laser irradiation under fluences around the ablation threshold. The Si-XII/III ratio across the rastered surface is 2.5 ± 0.5 .

Next, we characterize crystalline silicon polymorph formation in a laser-irradiated spot that received 88 stationary pulses with a peak fluence of 4 kJ/m^2 ; a representative spectrum is shown in (Figure 2(c)). The stationary spot received more high-fluence irradiation, which is reflected in the larger size of the surface peaks in the center of the stationary laser spot (Figure 2(d), inset) compared with the rastered surface (Figure 2(b), inset). The overall intensity of the silicon polymorph Raman modes, however, decreases dramatically compared to the rastered surface. Here we note that the observed differences in surface morphology between these two samples can slightly influence the measured Si-XII mode intensities, but this cannot account for the observed order-of-magnitude differences. In a line scan across the laser-irradiated spot (Figure 2(d)), small volumes of Si-XII can be detected $200\text{--}300 \mu\text{m}$ away from the center of the laser beam, but their average Raman mode intensities are an order of magnitude lower than what is observed on the rastered surface (2000 a.u. for the stationary spot vs. $>20\,000$ a.u. in the spectrum from the rastered surface). In this sample, no Si-III was detected above the noise limit (1500 a.u.).

Understanding the radial dependence of Si-XII formation in the stationary laser spot helps with elucidating the mechanism of drastic enhancement of Si-XII formation during laser rastering and, ultimately, identify the pressure-generation mechanism responsible for the observed phase transformations. There are a couple of possible causes of the observed radial dependence: (1) The radial distribution of Si-XII in the stationary spot is directly related to the fluence received at each point or (2) it is a consequence of a radial-dependence in the pressure generation across the entire laser-irradiated spot. In our investigations we irradiated a series of spots with 88 pulses at constant peak fluence, ranging from 4 kJ/m^2 to less than 2.0 kJ/m^2 . Here only the spots irradiated with a peak fluence of 4.0 kJ/m^2 spot and 3.2 kJ/m^2 (Figure 3) are compared, as these reflect all significant trends.

We begin by expanding the Raman line scan presented in Figure 2(d) to a 2D map of Si-XII formation across the entire laser spot. Figure 3(a) shows the laser-irradiated spot that received 88 pulses with $F_0 = 4.0 \text{ kJ/m}^2$ and the corresponding Si-XII map is shown in Figure 3(b). The spatial distribution of Si-XII formation can be correlated with the local fluence using Eq. (1), as labeled in Figure 3(b). The Si-XII Raman mode appears in an annulus that corresponds to fluences between 1.6 kJ/m^2 and 3.2 kJ/m^2 , whereas the Si-XII signal is suppressed in the region that received fluences greater than $\sim 3.2 \text{ kJ/m}^2$. Next, a spot was irradiated with 88 pulses at a peak fluence of 3.2 kJ/m^2 (Figure 3(c)), roughly equal to the upper fluence threshold for Si-XII formation observed in the $F_0 = 4.0 \text{ kJ/m}^2$ irradiated spot. The 2D map of the 3.2 kJ/m^2 laser spot (Figure 3(d)) shows no Si-XII suppression in the middle of the irradiated spot and the region of detectable Si-XII extends out to a fluence of

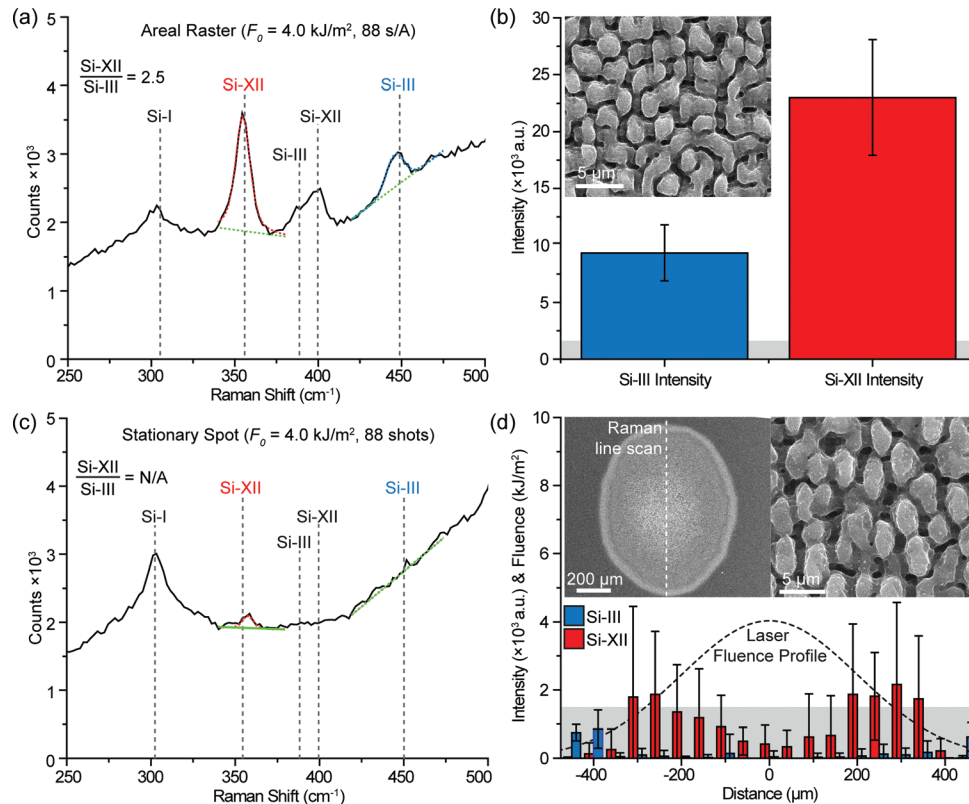


FIG. 2. (a) A representative Raman spectrum from a rastered surface that received 88 s/a with a peak fluence, F_0 , of 4 kJ/m^2 . The background (green) and fits to the Si-XII mode (red) and the Si-III mode (blue) are overlaid. (b) The average intensity and standard deviation of the Si-III (blue) and Si-XII (red) Raman modes from 20 spectra collected from the rastered surface; SEM image of the surface morphology is shown in inset. (c) A representative Raman spectrum from a stationary laser-irradiated spot that received 88 pulses with a peak fluence of 4 kJ/m^2 , with background (green) and a fit to the Si-XII mode (red) overlaid. The Si-III mode is not detectable. The spectrum corresponds to the position $300 \mu\text{m}$ from the center of the laser spot. (d) The average intensity and standard deviation of the Si-III and Si-XII Raman mode intensity measured across the stationary laser-irradiated spot (left inset) along with the varying laser fluence. The surface morphology at the center of the laser-irradiated spot is shown in the right inset. Line scans were obtained across 5 different laser spots and then spatially binned to illustrate trends. In both (b) and (d), the error bars represent one standard deviation and the gray regions indicate the peak fitting noise floor (1500 a.u.).

roughly 1.9 kJ/m^2 ; a threshold similar to what we observed for the 4.0 kJ/m^2 laser spot. Notably, we observe the same trends in further investigations of Si-XII formation following 88 pulses with $F_0 \leq 3.2 \text{ kJ/m}^2$ (not shown). Investigating the radial distribution of Si-XII formation confirms that Si-XII formation during stationary laser irradiation is a function of the fluence, and allowed us to identify an upper-and lower-fluence bound on the formation of Si-XII following irradiation with 88 laser pulses.

B. Effect of laser fluence modulation on silicon polymorph formation

Investigations of the relationship between laser irradiation conditions and pressure-induced phase transformations reveals that the act of rastering the laser beam across the surface drastically enhances the formation of crystalline silicon polymorphs compared to stationary-beam irradiation with constant fluence (Figure 2), regardless of the fluence received at the surface. The rastering of a Gaussian fs-laser beam (Figure 1(c)) delivers a range of fluences onto the same area, whereas irradiation with a stationary laser beam and fixed peak intensity does not have the same effect (Figure 1(a)). Hence, we next investigated the effect of fluence

modulation on the formation of Si-XII and Si-III by irradiating silicon with a stationary laser beam, but with varying peak fluences that mimic the irradiation dose received during laser rastering.

Figure 4(a) illustrates the irradiation conditions for the five samples investigated (FM1–FM5), allowing for visual comparison of the irradiation conditions with those created during laser rastering (Figure 1(b)). Sample FM5 received a range of fluences ($4.0\text{--}1.6 \text{ kJ/m}^2$) in proportions that emulate the total dosage received by a single point on a rastered surface. We note, however, that these conditions do not capture the oscillations in fluence or the large amount of irradiation with fluences $< 1.6 \text{ kJ/m}^2$ characteristic of laser rastering. Samples FM1–FM4 received only a portion of the fluence series, allowing us to understand the effect of each stage of irradiation on the formation of crystalline silicon polymorphs. Figure 4(b) shows the average Si-XII Raman mode intensities extracted from the center of each laser-irradiated spot. There is no detectable Si-XII mode in FM1, FM2, or FM3, which correspond to the first 25 laser pulses and cover the fluence range from $4.0\text{--}3.2 \text{ kJ/m}^2$. Irradiation with 12 subsequent pulses at 2.8 kJ/m^2 (FM4) causes an increase of the Si-XII signal to just around the noise limit (1500 a.u.). Similar to the constant fluence studies, there is no Si-III

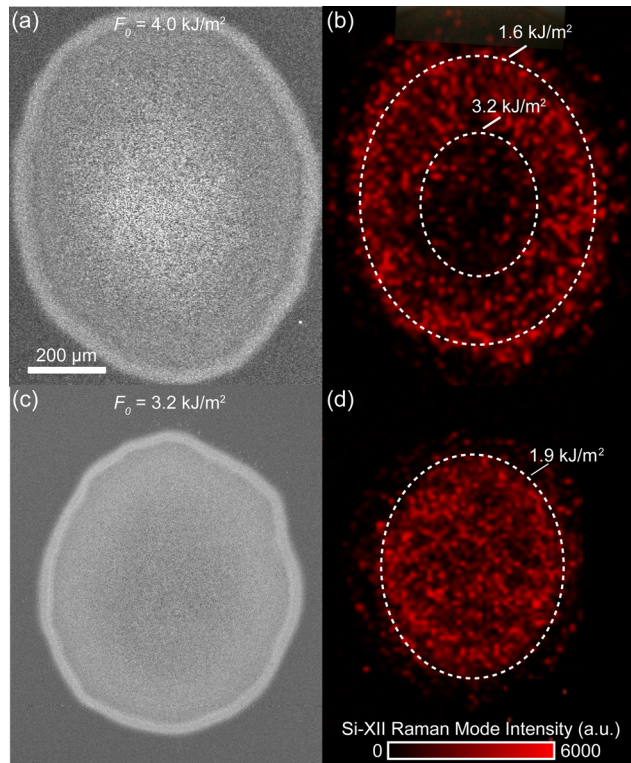


FIG. 3. (a) SEM image of a laser-irradiated spot that received 88 fs-laser pulses with a peak fluence, F_0 , of 4.0 kJ/m^2 . (b) Intensity of the Si-XII Raman mode mapped across the laser-irradiated spot shown in (a). Fluence thresholds for Si-XII detection are labeled. (c) SEM image of a laser-irradiated spot which received 88 fs-laser pulses with a peak fluence, F_0 , of 3.2 kJ/m^2 . (d) Intensity of the Si-XII Raman mode mapped across the laser-irradiated spot shown in (b). All SEM images and Raman maps are shown at the same scale and the color scale for both (b) and (d) are the same (shown in (d)).

signal detected in FM1–FM4. In the final stage of low-fluence irradiation (FM5), after 20 pulses at 2.4 kJ/m^2 , 12 at 2 kJ/m^2 , and 20 at 1.6 kJ/m^2 , we observe an increase in the intensity of the Si-XII mode to levels 4-times higher than achieved by irradiation with a similar number of laser pulses at any constant fluence. In addition, in FM5 the Si-III mode increases to levels above the noise limit. FM5 exhibits a Si-XII/III ratio of 4.5 ± 2.1 , higher than observed on the rastered surface (2.5 ± 0.5), indicating a stronger preference for Si-XII formation in FM5. The evolution of the surface morphology with increasing irradiation is shown in Figure 4(c). There is no noticeable difference in surface morphology between FM4 and FM5, indicating that irradiation with fluences in the range $1.6\text{--}2.4 \text{ kJ/m}^2$, as received by FM5 but not FM4, does not play a large role in surface texturing despite its evident role in driving Si-XII formation. Although the fluence profile on a rastered surface (Figure 1(b)) is much more complex than the fluence-modulated simulation (Figure 4(a)), this crude approximation demonstrates the role of fluence modulation during laser rastering in driving the formation of Si-XII.

In order to elucidate the relationship between fluence modulation and silicon polymorph formation, we use TEM to investigate the microstructure of FM4 (Figure 5(a)) and FM5 (Figure 5(b)). Specifically, TEM allows us to gain insight into both the amount of melting on the surface and

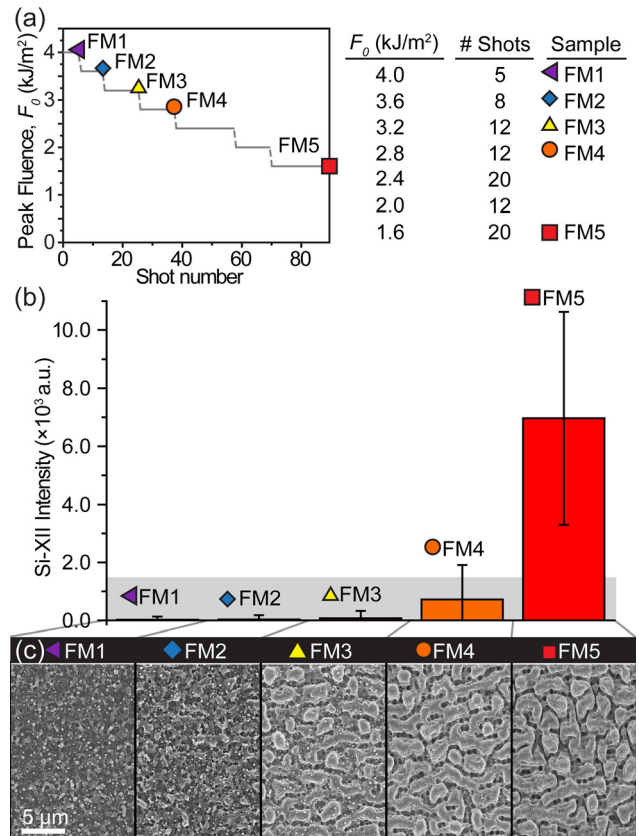


FIG. 4. (a) Irradiation conditions used to prepare fluence-modulated series, presented in a fluence-shot number plot for comparison with Figure 1. Details of fluence and pulse number are provided in the table (right). (b) Average Si-XII Raman mode intensity in the center $250 \mu\text{m}$ of each laser spot, reflecting 150 Raman spectra collected from each sample. Gray region ($<1500 \text{ a.u.}$) indicates the noise floor for peak fitting. (c) SEM images showing the surface morphology in the center of each laser-irradiated spot.

the spatial distribution of pressure-induced regions of amorphous silicon. Both FM4 and FM5 show an amorphous silicon layer on the surface, caused by melting and ultrafast resolidification, as well as regions of amorphous silicon forming beneath the melt depth, arising due to pressure-induced phase transformations. The amorphous regions beneath the melt depth have been thoroughly characterized in previous investigations¹⁶ and, consistent with those investigations, are seen here to form only in the core of the peaks. The appearance of amorphous silicon only in the core of the peaks indicates that the pressure generated at the surface is inhomogeneous and closely related to surface morphology. Measuring the depth of the resolidified amorphous layer on the surface provides insights into the extent of melting on the surface and its relationship with irradiation conditions (the increased amount of low-fluence irradiation delivered to FM5). The average thickness of the amorphous layer was measured across the entire width of the TEM sample and it reveals that the melt depth is $50 \pm 20 \text{ nm}$ and $70 \pm 30 \text{ nm}$ in FM4 and FM5, respectively (additional TEM characterization is provided in supplementary material).⁴³ From these results, we conclude that the additional low fluence irradiation received by FM5 increased the amount of amorphous silicon on the surface and therefore the amount of melting.

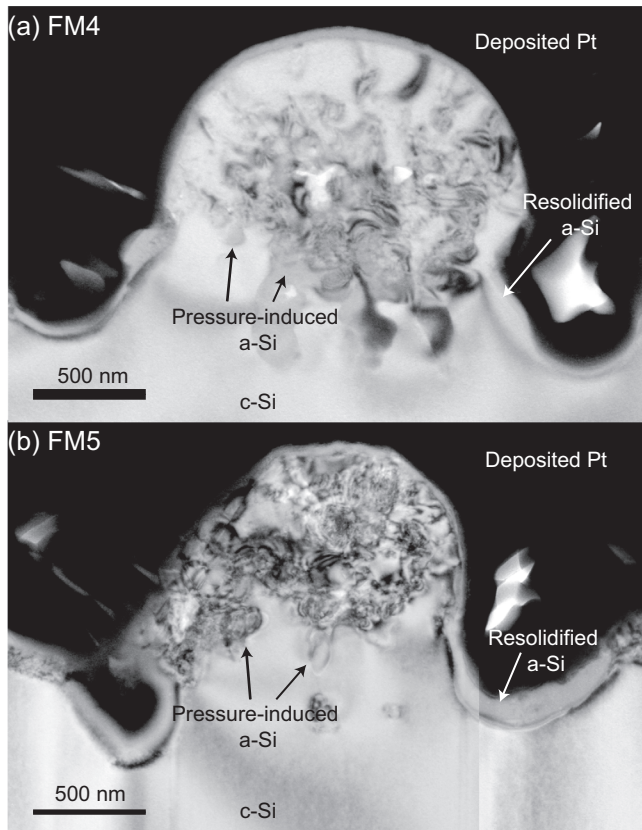


FIG. 5. Representative cross-sectional TEM images showing the microstructure of (a) FM4 and (b) FM5 samples (see supplementary material for more information). The amorphous silicon layer on the surface forms through melting and ultra-fast resolidification. Pressure-induced amorphous silicon regions 100–200 nm in size form beneath the surface. These are difficult to be individually resolved due to overlapping of amorphous silicon regions and the large amount of strain contrast in the surrounding c-Si matrix.

IV. DISCUSSION

A. Pressure-generation mechanisms driving phase transformations

Our investigations show that the formation of Si-XII and Si-III is enhanced by the act of rastering a Gaussian fs-laser beam across the surface, and that 88 stationary pulses at constant peak fluence (up to 4 kJ/m^2) consistently produce Si-XII at levels an order of magnitude lower than is achieved through laser rastering. The relatively low amounts of Si-XII detected in any constant-fluence laser-irradiated spot indicate that there are additional effects at play during laser rastering (beyond a straight-forward fluence dependence) that favor the formation of crystalline silicon polymorphs. We find that a stationary spot textured by high fluence irradiation ($4.0\text{--}2.8 \text{ kJ/m}^2$) followed by low fluence irradiation ($2.4\text{--}1.6 \text{ kJ/m}^2$) resulted in a 4-fold increase in Si-XII formation compared to samples irradiated with the same number of pulses at a fixed fluence. Finally, structural investigations show that the low fluence irradiation increases the thickness of the resolidified amorphous silicon layer on the surface (Figure 5), and that pressure-induced amorphous silicon forms only in the protruding surface peaks.

Combined with the previous review of pressure generation mechanisms during fs-laser irradiation, this investigation

of the relationship between silicon polymorph formation, irradiation conditions, and microstructure provides strong evidence that pressure-induced phase transformations are driven by resolidification-induced stresses. First, the increased depth of a-Si following irradiation at low fluences (comparing FM4 with FM5) reflects increased melting at the surface, and can be understood to arise due to the lower latent heat of melting of amorphous silicon compared to crystalline silicon.³⁴ Less energy is required to melt a layer of silicon that is initially amorphous, which results in a slight increase in the amount of material that melts on the surface with repeated irradiation. This process is prevalent only below the ablation threshold, because above the ablation threshold molten material is ejected from the surface. Rastering the laser beam delivers a large quantity of low-fluence irradiation, which drastically affects the amount of melting and resolidification at the surface.

Second, the appearance of pressure-induced amorphous silicon only within the core of the spikes on the surface (Figure 5) suggests that surface texturing plays an important role in driving pressure-induced phase transformations. The relationship between surface morphology, the spatial distribution of pressure-induced a-Si, and resolidification-induced stresses can be elucidated by referring to finite element modeling of residual surface stresses of Borowiec *et al.* in a 1-D trench due to cooling of a surface layer with a negative thermal expansion coefficient.³⁵ The negative thermal expansion coefficient is qualitatively accurate for silicon because silicon expands upon solidification.³⁶ This model predicts that volume expansion of a thin molten layer induces tensile stresses at the bottom of the trench and compressive stresses on the sides of the trench. We observe regions of amorphous silicon resulting from compressive stresses only in the protruding surface peaks (Figure 5), which one would expect to be under compression based on extrapolation of Borowiec's model. Previous investigations suggest that the crystalline silicon polymorphs form in the same regions as the sub-surface amorphous silicon, though their relatively small volume and metastability makes the crystalline silicon polymorphs difficult to detect by TEM.¹⁶ In addition, the valleys between the peaks—predicted by Borowiec's model to be under tensile stress—do not show any signs of plastic deformation and are composed entirely of Si-I. The hypothesis that resolidification-induced stresses are responsible for driving pressure-induced phase transformations beneath the surface is therefore further supported by the observed agreement between the spatial distribution of the pressure-induced phase transformations and the predicted relationship between surface morphology, resolidification, and the distribution of compressive and tensile stresses.

Finally, we find further support for the role of resolidification-induced pressures on sub-surface phase transformations by reviewing the sensitivity of silicon polymorph formation on the surrounding environment in the framework of the current understanding about the pressure generation mechanisms during fs-laser irradiation. The formation of Si-XII and Si-III depends strongly on both the rate of pressure unloading³⁷ and the surrounding temperature.³⁸ The formation of Si-XII and Si-III, which we observe in small amounts during fs-laser surface texturing, is kinetically

suppressed at pressure release rates on the order of microseconds.¹⁸ This time scale is orders of magnitude slower than most pressure-generation mechanisms associated with fs-laser irradiation. For example, the timescale of both thermoelastic pressure cycles and recoil shock waves are on the order of picoseconds, and thus, would be expected to inhibit the formation of Si-XII and Si-III.^{24,39} The intensity of recoil shock waves arising from the ejection of an ionic plasma decays so rapidly that the waves are capable of quenching Si-II and other high pressure phases, kinetically inhibiting even the formation of amorphous silicon upon pressure release.²⁶ The pressure loading arising due to resolidification of molten silicon on a roughened surface occurs on the same timescale as resolidification, which is on the order of nanoseconds.⁴⁰ The resolidification of molten silicon on a roughened surface, however, generates residual stresses beneath the surface in the GPa range.^{27,28} Based on the existence of large residual stresses, we can infer that pressure relaxation is frustrated and that the transient pressures may decay sufficiently slowly to allow for the nucleation of Si-XII. Thus, one would expect that resolidification-induced stresses are the most likely to allow for the nucleation of Si-XII, which agrees with the results presented in this paper.

B. Effects of the temperature dependence of plastic deformation mechanisms in silicon

The pressure-induced phase transformations in silicon are sensitive not only to pressure unloading rate but also to temperature, and thus, studying the formation of a-Si, Si-XII, and Si-III allows us to comment on the impact of irradiation conditions on local temperature and plastic deformation mechanisms. Femtosecond laser irradiation has a relatively small thermal footprint compared to longer pulse irradiation, but thermal effects are not completely absent. First, irradiation at fluences well below the melting threshold still results in moderate annealing at the surface. The fluence modulated sample (FM5) received 12 pulses at 2 kJ/m^2 and 20 pulses at 1.6 kJ/m^2 , while an 88 s/a areal raster delivers about 400 pulses in the range $0.1\text{--}2 \text{ kJ/m}^2$ (Figure 1(d)). This drastic difference in the amount of the received low-fluence irradiation can explain the observed difference in Si-XII/III ratio between FM5 and the areal raster. Only very modest temperatures ($100\text{--}200^\circ\text{C}$) are necessary to drive the Si-XII \rightarrow Si-III transition,⁴¹ decreasing the Si-XII/III ratio. Accordingly, the fluence modulated sample (FM5) exhibits a much higher Si-XII/III ratio (4.5 ± 2.1) than what was observed following an areal raster (2.5 ± 0.5). The lower relative concentration of Si-XII in the rastered surface could therefore be attributed to the large amount of low-fluence irradiation that the rastered sample receives.

Studies of the fs-laser heat affected zone have shown that temperature increases of several hundred $^\circ\text{C}$ can occur at micrometers beneath the surface following during fs-laser irradiation around the ablation threshold.⁴² Temperature increases on this order are sufficient to influence the dominant plastic deformation mechanisms in silicon. The Si-I \rightarrow Si-II phase transformation is the preferred mechanism of plastic deformation in silicon only at temperatures below

350°C , and Si-XII does not form at temperatures above 200°C .³⁸ Above 350°C , silicon becomes much softer due to thermally-enhanced dislocation glide and no phase transformations occur. The suppression of Si-XII formation under constant-fluence irradiation at fluences greater than 3.2 kJ/m^2 (Figure 3) could be a result of the temperature dependence of crystalline silicon polymorph formation. This suggests that 3.2 kJ/m^2 is the fluence threshold (at 88 pulses) below which the temperature stays sufficiently low to allow for the nucleation of Si-XII. The observation that the laser irradiation conditions affect the plastic deformation mechanisms due to their temperature dependence could have wide-reaching consequences, as additional processing parameters such as the environment (vacuum vs. ambient pressures) and laser pulse frequency could also affect the plastic deformation mechanisms in silicon via their effect on temperature.

V. CONCLUSIONS

In this paper, we investigated the mechanisms driving pressure-induced phase transformations during the surface texturing of silicon with fs-laser irradiation. Micro-Raman spectroscopy, SEM, and TEM characterization of samples irradiated under stationary and rastering conditions show that the resolidification of molten silicon on a textured surface plays a central role in driving sub-surface pressure-induced phase transformations. We show that this process is enhanced by the fluence modulation created by rastering a Gaussian laser beam across the surface, making this finding especially important for the application of fs-laser irradiation to large-scale surface treatments. Understanding that sub-surface plastic deformation is driven by resolidification-induced stresses (and not ablation) informs minimizing laser-induced damage by optimizing irradiation conditions to reduce resolidification-induced stresses. For example, it will be valuable to understand the effects of using higher-fluence irradiation to texture the surface, modifying the laser intensity profile (e.g., a flat-top intensity profile), and tuning rastering conditions to minimize low-fluence irradiation delivered during large-area surface texturing. We also show that the low-fluence irradiation received during the rastering of a Gaussian laser beam drives Si-III formation due to local annealing. This finding illustrates the effects of optical annealing using low fluence irradiation and suggests that careful design of the irradiation conditions could be used to incorporate an annealing step in parallel with laser rastering. Finally, this work suggests that the temperature dependence of the plastic deformation mechanisms in silicon likely influences the relationship between irradiation conditions and laser-induced modification.

ACKNOWLEDGMENTS

This work was supported by the Chesonis Family Foundation, the NSF ERC-QESST (EEC-1041895), and NSF Award Nos. CBET 0754227 and CHE-DMR-DMS 0934480. This research was also made with additional support through the National Defense Science and Engineering Graduate (NDSEG) Fellowship, 32 CFR 168a, and the R. J. McElroy

Trust. We acknowledge valuable use of MIT CMSE Shared Experimental Facilities, under MIT NSF MRSEC Grant No. DMR-08-19762, and the Harvard Center for Nanoscale Systems (CNS), a member of the National Nanotechnology Infrastructure Network (NNIN), which is supported by the National Science Foundation under NSF Award No. ECS-0335765.

- ¹M.-J. Sher, M. T. Winkler, and E. Mazur, *MRS Bull.* **36**, 439 (2011).
- ²B. K. Nayak, V. V. Iyengar, and M. C. Gupta, *Prog. Photovoltaics* **19**, 631 (2011).
- ³R. Torres, V. Vervisch, M. Halbwax, T. Sarnet, P. Delaporte, M. Sentis, J. Ferreira, D. Barakel, S. Bastide, F. Torregrosa, H. Etienne, and L. Roux, *J. Optoelectron. Adv. Mater.* **12**, 621 (2010).
- ⁴C. Vineis, M. Levy-Finklshtein, J. E. Carey, G. Knight, E. Wefringhaus, and R. Harney, in *InterPV*, December 2011.
- ⁵B. R. Tull, J. E. Carey, E. Mazur, J. McDonald, and S. M. Yalisove, *Mater. Res. Soc. Bull.* **31**, 626–633 (2006).
- ⁶M. Smith, M. Winkler, M.-J. Sher, Y.-T. Lin, E. Mazur, and S. Gradečak, *Appl. Phys. A: Mater. Sci. Process.* **105**, 795 (2011).
- ⁷C. H. Crouch, J. E. Carey, M. Shen, E. Mazur, and F. Y. Génin, *Appl. Phys. A: Mater. Sci. Process.* **79**, 1635 (2004).
- ⁸M. T. Winkler, D. Recht, M.-J. Sher, A. J. Said, E. Mazur, and M. J. Aziz, *Phys. Rev. Lett.* **106**, 178701/1 (2011).
- ⁹E. Ertekin, M. T. Winkler, D. Recht, A. J. Said, M. J. Aziz, T. Buonassisi, and J. C. Grossman, *Phys. Rev. Lett.* **108**, 026401 (2012).
- ¹⁰J. E. Carey, C. H. Crouch, M. Shen, and E. Mazur, *Opt. Lett.* **30**, 1773 (2005).
- ¹¹N. López, L. A. Reichertz, K. M. Yu, K. Campman, and W. Walukiewicz, *Phys. Rev. Lett.* **106**, 028701 (2011).
- ¹²K. Sánchez, I. Aguilera, P. Palacios, and P. Wahnón, *Phys. Rev. B* **82**, 165201 (2010).
- ¹³S. H. Zaidi, D. S. Ruby, and J. M. Gee, *IEEE Trans. Electron Devices* **48**, 1200 (2001).
- ¹⁴S. Schaefer and R. Ludemann, *J. Vac. Sci. Technol. A* **17**, 749 (1999).
- ¹⁵M. Otto, M. Kroll, T. Kasebier, R. Salzer, A. Tunnermann, and R. B. Wehrspohn, *Appl. Phys. Lett.* **100**, 191603 (2012).
- ¹⁶M. J. Smith, Y.-T. Lin, M.-J. Sher, M. T. Winkler, E. Mazur, and S. Gradečak, *J. Appl. Phys.* **110**, 053524 (2011).
- ¹⁷R. Hull (chapter editor), “Structural and mechanical properties,” in *Properties of Crystalline Silicon*, edited by A. George (INSPEC, London, UK, 1999), Chap. 3.
- ¹⁸S. Ruffell, J. E. Bradby, and J. S. Williams, *Appl. Phys. Lett.* **89**, 091919 (2006).
- ¹⁹J. Crain, G. J. Ackland, J. R. Maclean, R. O. Piltz, P. D. Hatton, and G. S. Pawley, *Phys. Rev. B* **50**, 13043 (1994).
- ²⁰J.-I. Jang, M. J. Lance, S. Wen, T. Y. Tsui, and G. M. Pharr, *Acta Mater.* **53**, 1759 (2005).
- ²¹Q. Feng, Y. N. Picard, H. Liu, S. M. Yalisove, G. Mourou, and T. M. Pollock, *Scr. Mater.* **53**, 511 (2005).
- ²²S. Schoenfelder, J. Bagdahn, S. Baumann, D. Kray, K. Mayer, G. Willeke, M. Becker, and S. Christiansen, “Strength characterization of laser diced silicon for application in solar industry,” in *Proceedings of the 21st European Photovoltaic Solar Energy Conference*, Dresden, Germany, 4–8 Sept., 2006, pp. 588–592.
- ²³K. Sokolowski-Tinten, J. Bialkowski, A. Cavalleri, D. von der Linde, A. Oparin, J. Meyer-ter-Vehn, and S. I. Anisimov, *Phys. Rev. Lett.* **81**, 224 (1998).
- ²⁴D. Perez and L. J. Lewis, *Phys. Rev. B* **67**, 184102 (2003).
- ²⁵T. Sano, K. Takahashi, A. Hirose, O. Sakata, M. Okosh, N. Inoue, and K. F. Kobayashi, in *PRICM 6*, edited by Y. W. Chang, N. J. Kim, and C. S. Lee (Trans Tech Publications Ltd, Stafa-Zurich, 2007), Vol. 561–565, p. 2349.
- ²⁶M. Tsujino, *Rev. Laser Eng.* **36**, 1218 (2008).
- ²⁷M. S. Amer, L. Dosser, S. LeClair, and J. F. Maguire, *Appl. Surf. Sci.* **187**, 291 (2002).
- ²⁸A. Borowiec, M. Couillard, G. A. Botton, and H. K. Haugen, *Appl. Phys. A: Mater. Sci. Process.* **79**, 1887 (2004).
- ²⁹J. Bonse, S. Baudach, J. Krüger, W. Kautek, and M. Lenzner, *Appl. Phys. A: Mater. Sci. Process.* **74**, 19 (2002).
- ³⁰A. Cavalleri, K. Sokolowski-Tinten, J. Bialkowski, M. Schreiner, and D. von der Linde, *J. Appl. Phys.* **85**, 3301 (1999).
- ³¹D. P. Korfiatis, K. A. T. Thoma, and J. C. Vardaxoglou, *J. Phys. D: Appl. Phys.* **40**, 6803 (2007).
- ³²Y. Jee, M. F. Becker, and R. M. Walser, *J. Opt. Soc. Am. B* **5**, 648 (1988).
- ³³M. T. Winkler, Ph.D dissertation, Harvard University, 2009.
- ³⁴F. Falk and G. Andrä, *J. Cryst. Growth* **287**, 397 (2006).
- ³⁵A. Borowiec, D. M. Bruce, D. T. Cassidy, and H. K. Haugen, *Appl. Phys. Lett.* **83**, 225 (2003).
- ³⁶M. R. Brozel (chapter editor), “Thermal properties,” *Properties of Crystalline Silicon*, 1st ed., edited by A. George (INSPEC, London, UK, 1999), Chap. 4.
- ³⁷S. Ruffell, J. E. Bradby, J. S. Williams, and P. Munroe, *J. Appl. Phys.* **102**, 063521 (2007).
- ³⁸V. Domnich, Y. Aratyn, W. M. Kriven, and Y. Gogotsi, *Rev. Adv. Mater. Sci.* **17**, 33 (2008).
- ³⁹R. Evans, A. D. Badger, F. Falliès, M. Mahdich, T. A. Hall, P. Audebert, J. P. Geindre, J. C. Gauthier, A. Mysyrowicz, G. Grillon, and A. Antonetti, *Phys. Rev. Lett.* **77**, 3359 (1996).
- ⁴⁰S. K. Sundaram and E. Mazur, *Nature Mater.* **1**, 217 (2002).
- ⁴¹S. Ruffell, B. Haberl, S. Koenig, J. E. Bradby, and J. S. Williams, *J. Appl. Phys.* **105**, 8 (2009).
- ⁴²Y. Li, W. Ching-Yue, and Y. Wei, *J. Phys: Conf. Ser.* **276**, 012032 (2011).
- ⁴³See supplementary material at <http://dx.doi.org/10.1063/1.4759140> for additional TEM characterization.